

First constraint on the dissipative tidal deformability of neutron stars

Justin L. Ripley,¹ Abhishek Hegade K.R.,¹ Rohit S. Chandramouli,¹ and Nicolás Yunes¹

¹*Illinois Center for Advanced Studies of the Universe & Department of Physics,
University of Illinois at Urbana-Champaign, Urbana, IL 61801, USA*

(Dated: December 20, 2023)

The gravitational waves (GWs) emitted by neutron star binaries provide a unique window into the physics of matter at supra nuclear densities. During the late inspiral, tidal deformations raised on each star by the gravitational field of its companion depend crucially on the star’s internal properties. The misalignment of a star’s tidal bulge with its companion’s gravitational field encodes the strength of internal dissipative processes, which imprint onto the phase of the gravitational waves emitted. We here analyze GW data from the GW170817 (binary neutron star) event detected by LIGO and Virgo and find the first constraint on the dissipative tidal deformability of a neutron star. From this constraint, *assuming* a temperature profile for each star in the binary, we obtain an order of magnitude bound on the averaged bulk (ζ) and shear (η) viscosity of each star during the inspiral: $\zeta \lesssim 10^{31} \text{ g cm}^{-1} \text{ s}^{-1}$ and $\eta \lesssim 10^{28} \text{ g cm}^{-1} \text{ s}^{-1}$. We forecast that this bound for the bulk (shear) viscosities could be improved to $10^{30} \text{ g cm}^{-1} \text{ s}^{-1}$ ($10^{27} \text{ g cm}^{-1} \text{ s}^{-1}$) during the fifth observing run of advanced LIGO and Virgo, and to $10^{29} \text{ g cm}^{-1} \text{ s}^{-1}$ ($10^{26} \text{ g cm}^{-1} \text{ s}^{-1}$) with third-generation detectors, like Cosmic Explorer, using inspiral data. These constraints already inform nuclear physics models and motivate further theoretical work to better understand the interplay between viscosity and temperature in the late inspiral of neutron stars.

Introduction. Neutron stars are the densest material objects in the universe, with their interior reaching densities many times that of atomic nuclei, at temperatures well below those probed by heavy ion collisions [1]. Determining the physical properties of neutron star matter, therefore, has remained an outstanding problem in the fields of astrophysics, gravitational physics, and nuclear physics for almost a century [2–4]. Gravitational waves from neutron star binaries encode the tidal deformations that neutron stars experience during their late inspiral before merger. These tidal deformations are in turn affected by the material properties of the stars. The prompt, conservative, relativistic tidal response is described by the tidal deformability Λ [5–7], which encodes aspects of the *equilibrium* properties of neutron star matter—the neutron star equation of state [3]. The gravitational waves from the binary neutron star event GW170817 allowed for the first constraints on the tidal deformability of neutron stars, and thus, for the first gravitational-wave (GW) inference on the equation of state [8, 9].

The tidal response of a star can be visualized as a “tidal bulge” that is sourced but not aligned with the time-varying, externally-imposed gravitational field of its companion. (see Fig. 1). Non-equilibrium, dissipative effects within the star force the bulge to trail the orbit, inducing a tidal lag angle between the direction of the bulge and the orbital separation. The extent to which the tidal multipolar moments are misaligned with the external gravitational multipolar moments is, to first approximation, described by the tidal lag time τ_d . The tidal lag time is a universal feature for self-gravitating astrophysical objects, from planets [10, 11] to black holes [12, 13], and it has been observed in many planetary systems [11, 14]. This tidal misalignment torques the two stars and heats them up through tidal, viscous heating (e.g. [15, 16]).

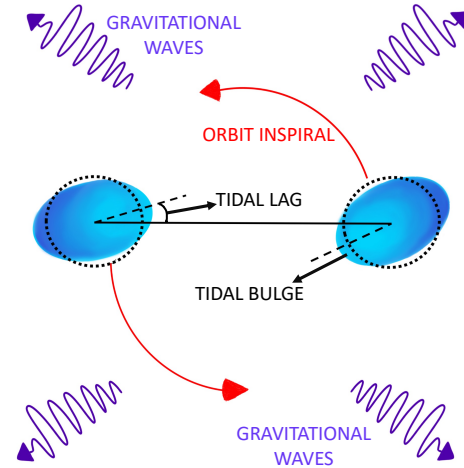


FIG. 1. Cartoon of the tidal responses of two stars in a quasi-circular binary (not to scale). Dissipative, out-of-equilibrium effects force the tidal bulge of each star to be misaligned with the gravitational field sourced by its companion.

The magnitude of these effects on the dynamics of neutron star binaries had been thought since the 1990s to be too small to measure with gravitational waves. Indeed, unphysically large values of viscosity are required to tidally lock the spins of the two stars to their orbit before merger [17]. Recent work in nuclear physics, however, suggests that weak-force processes can induce an effective bulk viscosity [18–25], which, although not large enough to tidally lock the spins of the two stars, may still have a measurable effect in the gravitational waves emitted during the late inspiral [26]. This has motivated different numerical groups to model out-of-equilibrium effects during the late inspiral, merger and the post-merger

phase. Some groups have found bulk viscous effects to be enhanced during the late inspiral [21, 27, 28]. Meanwhile, other groups working with moment-based treatments of neutrino transport have not found evidence for large out-of-thermodynamic equilibrium effects necessary for producing an effective bulk viscosity during the late inspiral [29]. Nevertheless, these moment-based treatments of neutrino transport have revealed evidence of bulk viscous effects within a small window after the merger before matter goes back to equilibrium [30]. Given these differences in literature it is crucial to utilize the available gravitational wave data to provide insights into out-of-equilibrium effects present during the late inspiral and merger phase.

Recently, the signature of the tidal lag in the gravitational waves emitted by binary neutron star inspirals was re-analyzed in [26], and found to be parametrically enhanced relative to that of conservative tidal effects. Conservative tidal effects first enter the GW phase proportional to ten powers of the orbital velocity relative to the leading-order term in a small-velocity, post-Newtonian expansion, which in the late inspiral is $v \sim (0.25\text{--}0.4)c$; moreover, conservative effects are inversely proportional to five powers of the stellar compactness, i.e. the dimensionless ratio of its mass to its radius, which for neutron stars is $C \sim 0.1\text{--}0.3$ [5, 31]. In contrast, dissipative tidal effects first enter the GW phase proportional to eight powers of the orbital velocity and inversely proportional to six powers of the stellar compactness [26]. Therefore, this parametric enhancement boosts the effect of dissipative tidal effects, making them potentially measurable with *current* ground-based GW detectors for physically plausible levels of dissipation within the stars.

The contribution of the tidal lag to the GW phase is captured by the dissipative counterpart to the conservative tidal deformability Λ : the dissipative tidal deformability Ξ , which can be mapped to the effective bulk/shear viscosities of the star [26, 32]. Large values of bulk viscous dissipation could be sourced through Urca processes [18, 19, 21, 23], or more exotic nuclear processes due to the presence of hyperons deep in the interior of a neutron star [33–36]. This effective viscosity depends on the particular nuclear and fluid models used, on the equation of state of the star, and on its temperature. Therefore, a measurement or constraint on Ξ cannot be translated to an independent measurement or constraint of any single one of these ingredients, without an assumption about the values of any two of the other quantities. Nonetheless, taking the expected values for these quantities, a preliminary forecast in [26] suggested that the total extent of dissipative processes within neutron stars could be meaningfully constrained through an analysis of current GW data. We here carry out precisely such an analysis and find the first constraints on the dissipative tidal deformability of neutron stars using data from the GW170817 event detected by LIGO and Virgo [8].

Gravitational-wave model with conservative and dissipative tidal effects. We use a state-of-the-art model for the detector response to the impinging gravitational waves emitted in the inspiral of binary neutron star (i.e., the so-called `IMRPhenomPv2_NRTidal` waveform model [37]), which we enhance to include tidal dissipation. In the frequency domain, we represent the model via the Fourier transform of the GW strain $\tilde{h}(f) = A(f) e^{i\Psi(f)}$, where $A(f)$ is the Fourier GW amplitude and $\Psi(f)$ is the Fourier GW phase. Without tidal dissipation, the `IMRPhenomPv2_NRTidal` model depends on 17 parameters θ_a , which, in addition to the non-tidal ones (such as the chirp mass $\mathcal{M} \equiv m_A^{3/5} m_B^{3/5} / M^{1/5}$ and the symmetric mass ratio $\eta_{\text{sym}} \equiv m_A m_B / M^2$, with $M \equiv m_A + m_B$ the total mass and $m_{A/B}$ the component masses; see the Supp. Mat. for more details), includes the tidal deformabilities of the stars $\Lambda_{A/B}$.

We enhance the `IMRPhenomPv2_NRTidal` model by adding the leading post-Newtonian contribution of the dissipative tidal deformability to the `IMRPhenomPv2_NRTidal` Fourier phase [26]

$$\Psi(f; \theta) = \Psi_{\text{Pv2NRT}}(f; \theta_a) - \frac{225}{4096} \frac{1}{\eta_{\text{sym}}} \bar{\Xi} u^3 \log(u), \quad (1)$$

where $u \equiv (G\pi M f / c^3)^{1/3}$ is effectively the orbital velocity. Since the leading, post-Newtonian order term in Ψ_{Pv2NRT} is proportional to u^{-5} , we see that the dissipative tidal contribution is of $\mathcal{O}(u^8)$ relative to leading order, which is of $\mathcal{O}(u^2)$ larger than the $\mathcal{O}(u^{10})$ relative conservative tidal contribution in Ψ_{Pv2NRT} . The quantity $\bar{\Xi}$ is the binary dissipative “chirp” tidal deformability. The parameter $\bar{\Xi}$ is a weighted sum of the dissipative tidal deformabilities of each star, $\Xi_{A,B}$

$$\begin{aligned} \bar{\Xi} \equiv & 8 (2\eta_{\text{sym}}^2 - 4\eta_{\text{sym}} + 1) \Xi_s \\ & - 8\sqrt{1 - 4\eta_{\text{sym}}} (1 - 2\eta_{\text{sym}}) \Xi_a, \end{aligned} \quad (2)$$

where $\Xi_s \equiv (\Xi_A + \Xi_B) / 2$ and $\Xi_a \equiv (\Xi_A - \Xi_B) / 2$. Therefore, the enhanced `IMRPhenomPv2_NRTidal` model contains 18 parameters: $\theta = \theta_a \cup \{\bar{\Xi}\}$.

Data analysis methodology. We use a Bayesian parameter estimation to compute the posterior probability distribution for all the parameters of our enhanced `IMRPhenomPv2_NRTidal` GW model, given 128s of the publicly available 4kHz GW170817 (glitch-cleaned) GW strain data [42]. We sample over all 18 parameters of the model and we marginalize over the reference phase. We validate our methodology by sampling both independently in $\Lambda_{A/B}$ and by using the binary love relations [38–41]. In the latter case, we marginalize over the uncertainty in the binary Love relations, following [40, 41]. As usual in GW data analysis, the likelihood is the noise model, which is assumed to be Gaussian and stationary [43, 44]; the log-likelihood is then (minus) one half of the (matched-filtering) inner-product magnitude of the

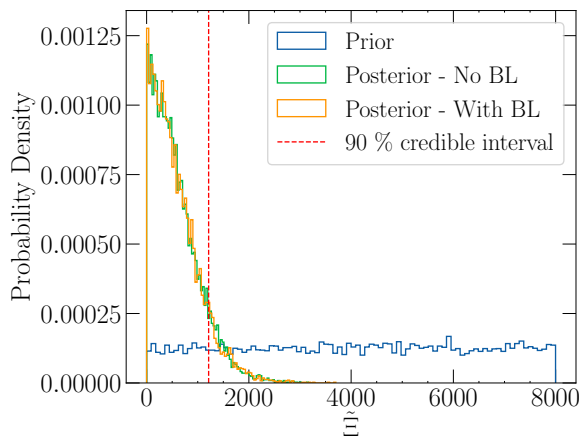


FIG. 2. Marginalized posterior distribution for $\bar{\Xi}$ for the GW170817 event with and without the marginalized binary Love relations [38–41], and the 90% credible interval. Observe that the GW170817 data is sufficiently informative to significantly constrain $\bar{\Xi}$ as compared to the prior, while remaining independent of the use of the binary Love relations.

difference between the data and the model. We use the Bilby [45] GW library, modified to incorporate the dissipative tidal effects of Eq. (1), and sample the likelihood with a nested sampling algorithm [46] as implemented in DYNesty [47] (see the Supp. Mat. for specific sampling details).

We choose the following priors for all our parameter estimation analysis. For all non-tidal waveform parameters, we choose the same priors as those employed by the LIGO-Virgo (LV) scientific collaboration during the analysis of the GW170817 event [9] (see also the Supp. Mat.). In particular, as the `IMRPhenomPv2_NRTidal` model does not include spin corrections to the conservative tidal effects¹, we use the “low-spin” prior defined in [9]. For the conservative tidal deformability, we use a uniform prior in $[0, 3000]$ for $\Lambda_{A,B}$, which implies a triangular prior for Λ_s when using the binary love relations. For the dissipative tidal deformability $\bar{\Xi}$, we choose a uniform prior in $[0, 8000]$. Our lower prior on $\bar{\Xi}$ is set to zero because we exclude the possibility of anti-dissipative processes within each star ($\Xi_A < 0$). The upper end of the prior on $\bar{\Xi}$ is set by a heuristic constraint on the timescale for causal momentum transport across the star: dissipative/viscous effects should not transport momentum faster than light speed [17, 26].

Analysis of the GW170817 event. Before analyzing the GW170817 data with the enhanced `IMRPhenomPv2_NRTidal` model, we validate our parameter estimation methodology by repeating the

LV analysis [9] with our data analysis implementation. As expected, we recover consistent posterior probability distributions for all the parameters of the `IMRPhenomPv2_NRTidal` model. We then analyze the GW170817 data with the enhanced `IMRPhenomPv2_NRTidal` model. We present the marginalized posterior distribution on $\bar{\Xi}$ from that analysis in Fig. 2. Observe that the data is informative, yielding a posterior that is significantly different than the prior and peaked at zero with $\bar{\Xi} < 1200$ at 90% confidence. Observe also that the posterior is independent of whether we use the marginalized binary Love relations or not. We deployed a number of tests to ensure the results of Fig. 2 are robust, which we describe in the Supp. Mat.

The marginalized posterior distributions for almost all other parameters are statistically consistent with those obtained by the LV collaboration when one does not include dissipative tidal effects. The one exception is the posterior for $\bar{\Lambda}$ (or equivalently for Λ_s or $\Lambda_{A,B}$), which are pushed to lower values due to correlations between the conservative and dissipative tidal deformabilities, as shown in Fig. 4 of the Supp. Mat. This implies that if the dissipative tidal deformability is present in the signal, and one neglects to incorporate its effects in the waveform model, one will then be biased in the estimation of the conservative tidal deformability to higher values than those contained in the signal.

Implications for nuclear physics. Any dissipative process within a neutron star adds cumulatively to the dissipative tidal deformability. As a consequence of this, an upper bound on $\bar{\Xi}$ constrains the strength of any given dissipative process.

Given a fluid model for the star, we can relate the dissipative tidal deformability to the tidal lag inside star A via [26]

$$\bar{\Xi}_A = \frac{2}{3} k_{2,A} \left(\frac{1}{C_A^6} \right) \left(\frac{c\tau_{d,A}}{R_A} \right), \quad (3)$$

where $k_{2,A}$ is the conservative tidal Love number of the star, m_A and R_A are the stellar mass and radius, $C_A \equiv Gm_A/(R_A c^2)$ is its compactness, and $\tau_{d,A}$ is its tidal lag time. The dissipative tidal deformability is parametrically enhanced by six inverse powers of the stellar compactness, which is one more inverse power than the parametric enhancement in the conservative tidal deformability Λ_A . We relate the tidal lag time to the viscosity via $\tau_{d,A} = p_{2,A} \langle \delta \rangle R_A c^2 / (Gm_A \langle e \rangle)$, where $\langle \delta \rangle = \langle \eta \rangle$ (the shear viscosity) or $\langle \zeta \rangle$ (the bulk viscosity) depending on which source of dissipation is dominant; $p_{2,A}$ is a dimensionless constant that is computed for a given viscosity profile $\delta(e)$, and $\langle e \rangle$ is the average energy density. Using that the conservative tidal deformability

¹ We note that our dissipative tidal term contains no spin corrections either.

$\Lambda_A \equiv (2k_{2,A}/3)/C_A^5$ [31], we then obtain

$$\begin{aligned} \Xi_A &= \frac{c^3}{G} \frac{p_{2,A} \Lambda_A}{C_A} \frac{\langle \delta \rangle}{\langle e \rangle m_A}, \\ &\approx 26.1 \times \left(\frac{p_{2,A}}{0.01} \right) \left(\frac{\Lambda_A}{300} \right) \left(\frac{0.188}{C_A} \right) \left(\frac{\langle \delta \rangle}{10^{30} \frac{\text{g}}{\text{cm}^3}} \right) \\ &\times \left(\frac{1.38 M_\odot}{m_A} \right) \left(\frac{9 \times 10^{34} \frac{\text{erg}}{\text{cm}^3}}{\langle e \rangle} \right). \end{aligned} \quad (4)$$

Characteristically, $p_{2,A} \sim 0.01$ when bulk viscosity drives the process of dissipation, but it can be as high as $p_{2,A} \sim 5$ when shear viscosity dominates [32]. This is because for the same magnitude of the coefficient of viscosity, shear viscosity couples more strongly to gravitational perturbations than the bulk viscosity does, as gravitational fields cause a larger relative shearing motion than compression of the star [32].

We can map the constraint we obtained on the dissipative tidal deformability to the microphysics of dissipative processes inside a neutron star if we make the following assumptions. Let us assume that both stars in the binary had the same equation of state and the same mass (which is consistent with the posterior for the GW170817 event). If so, they must also have the same compactness $C_A = C_B$ and the same the equation of state, and hence the same tidal deformability $\Lambda_A = \Lambda_B$. Let us further assume that both stars shared the same dissipative profile $\delta(e)$, so that the proportionality constants are equal, $p_{2,A} = p_{2,B}$ and the dissipative tidal deformabilities are equal, $\Xi_A = \Xi_B = \bar{\Xi}$. We then invert Eq. (4) to obtain

$$\begin{aligned} \langle \delta \rangle_A &\approx 4.6 \times 10^{31} \frac{\text{g}}{\text{cm s}} \times \left(\frac{\bar{\Xi}}{1200} \right) \left(\frac{\langle e \rangle}{9 \times 10^{34} \text{erg cm}^{-3}} \right) \\ &\times \left(\frac{300}{\Lambda_A} \right) \left(\frac{0.01}{p_{2,A}} \right) \left(\frac{C_A}{0.188} \right) \left(\frac{m_A}{1.38 M_\odot} \right). \end{aligned} \quad (5)$$

If shear viscosity was the dominant contribution to the dissipation, we would then obtain $\langle \eta \rangle \approx 9.15 \times 10^{28} \text{g cm}^{-1} \text{s}^{-1}$ with a normalization factor of $(5/p_{2,A})$ instead of $(0.01/p_{2,A})$. Given our measured bound of $\bar{\Xi} \lesssim 1200$, we can place an upper bound on the averaged bulk and shear viscosity during the evolution of the GW170817 event. We respectively obtain $\langle \zeta \rangle_A \lesssim 4.57 \times 10^{31} \text{g cm}^{-1} \text{s}^{-1}$ and $\langle \eta \rangle_A \lesssim 9.15 \times 10^{28} \text{g cm}^{-1} \text{s}^{-1}$.

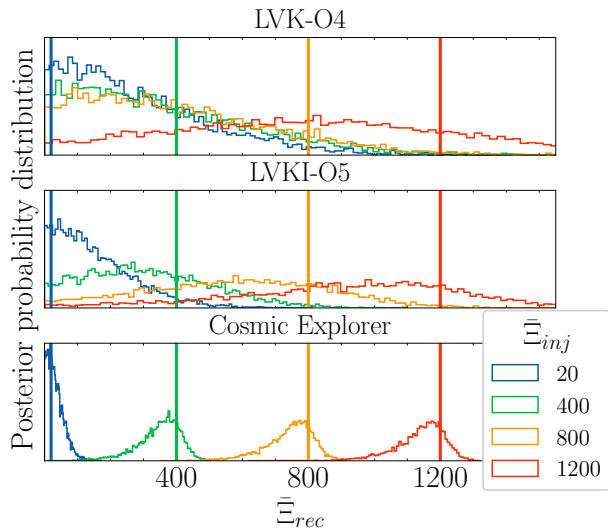
We now put this constraint in context by comparing it to current theoretical estimates of the viscosity of neutron stars. Viscosity generated by microscopic processes in neutron stars depends sensitively on the local stellar temperature profile T ; not only does T affect the theoretically predicted values of viscosity, but also the mechanism that drives dissipation. Shear viscosity in neutron cores scales as T^{-2} due to electron-muon scattering [48] and is expected to be less than $\langle \eta \rangle \lesssim 10^{22} \text{g cm}^{-1} \text{s}^{-1}$. Shear viscous contributions due to the interface of the stars crust with its interior have been speculated to be as large as $\langle \eta \rangle \sim 10^{29} \text{g cm}^{-1} \text{s}^{-1}$ [49]. Bulk viscous contributions due to the presence of hyperons can scale as T^{-2}

and may be the dominant source of dissipation in neutron stars at very low ($\sim \text{keV}$) temperatures, with values of bulk viscosity predicted to exceed $\langle \zeta \rangle \sim 10^{30} \text{g cm}^{-1} \text{s}^{-1}$ in some models [33–36]. As the binary enters the late inspiral, heating from tidal friction due to Urca reactions may increase the temperature of the two stars to tens of keV [16], with additional hyperonic bulk viscous contributions possibly heating the stars to higher temperatures [35]. Numerical relativity simulations of neutron star mergers suggest tidal heating could increase the stellar temperature to a few MeV during the last few orbits [50]. As the star’s temperature begins to increase, bulk viscous contributions from direct and modified Urca processes are expected to dominate because those reactions scale as T^4 and T^6 , respectively [18]². Typical predictions for the bulk viscosity for Urca-process-driven viscosity range from $\langle \zeta \rangle \sim 10^{26} \text{g cm}^{-1} \text{s}^{-1}$ when $T \sim 0.1 \text{MeV}$, to $\langle \zeta \rangle \sim 10^{31} \text{g cm}^{-1} \text{s}^{-1}$ when $T \sim 1 \text{MeV}$, depending on the equation of state [21, 23]. To estimate when temperature evolution is important, we perform an estimate of the number of GW cycles that $\bar{\Xi}$ introduces in different regimes of the inspiral. We estimate (see Supp. Mat.) that a $\bar{\Xi} \sim 1200$ introduces ~ 1.86 GW cycles over the last ~ 27 orbits (corresponding roughly to orbital separations from $\sim 83 \text{km}$ to contact), and a total of ~ 2.5 GW cycles over the entire inspiral. These result suggests that accounting for finite temperature and out-of-equilibrium effects in this last stage of the inspiral will be critical to get a more robust understanding of the underlying nuclear physics.

Future detectability of dissipative tides. We simulate synthetic GW detections for three different networks: ground-based detectors in the O4 and O5 era (i.e. the current LIGO observation run setup, and the following upgrade with the addition of the LIGO-India detector) [52], and the Cosmic Explorer (CE) era (one CE instrument at the current Hanford detector site) [53]. Each simulation consists of 128s of synthetic data, all starting at 40Hz; The component masses and the symmetric conservative tidal deformabilities in each simulation are kept fixed at $m_{A,B} = 1.38 M_\odot$ and $\Lambda_s = 584$ respectively, while the injected chirp dissipative tidal deformabilities are chosen to be $\bar{\Xi} = \{20, 400, 800, 1200\}$. The $m_{A,B}$ and Λ_s choices are consistent with the the marginalized posterior distribution of these parameters in the GW170817 event, and the $\bar{\Xi}$ choice is consistent with the constraint we obtained at 90% confidence. Since the luminosity distance is kept fixed, the signal-to-noise ratio (SNR) increases in the O4, O5, and CE simulations to ~ 60 , ~ 100 , and ~ 1100 , respectively.

² We note that beyond a resonant peak, these reactions become less strong at higher temperatures; current estimates place this peak at $T \sim 5 \text{MeV}$ [51], that is at higher temperatures than we expect the stars to reach during the inspiral.

We analyze these injections using Bayesian parameter estimation and our enhanced `IMRPhenomPv2_NRTidal` waveform model, following almost the same data analysis procedure as for the GW170817 event. The only difference is that, this time, we only sample on $\{\mathcal{M}, q, \Lambda_s, \bar{\Xi}\}$, and thus, we fix all other parameters in the posterior to their injected values; we find empirically that this does not qualitatively affect our conclusions. We emphasize that we use the same Uniform prior for $\bar{\Xi}$ that we use in our analysis of GW170817; that is we do not use our marginalized posterior for $\bar{\Xi}_A$ from GW170817 as our prior for $\bar{\Xi}$ in our injection runs. Figure 3 shows the marginalized



$\bar{\Xi}_{inj}$	$\bar{\Xi}_{MAP}^{(O4)}$	$\bar{\Xi}_{MAP}^{(O5)}$	$\bar{\Xi}_{MAP}^{(CE)}$
20	89^{+522}_{-88}	16^{+301}_{-16}	11^{+57}_{-11}
400	197^{+615}_{-197}	270^{+301}_{-270}	380^{+116}_{-123}
800	528^{+560}_{-528}	584^{+451}_{-541}	771^{+132}_{-132}
1200	803^{+704}_{-704}	974^{+584}_{-584}	1175^{+136}_{-145}

FIG. 3. (Top) Histograms of the marginalized posterior distributions for $\bar{\Xi}$ for zero-noise realizations of a GW170817-like event, simulated to be detected with the O4 LVK, O5 LVKI, and CE detector networks. The vertical lines represent the injected values of $\bar{\Xi}$. We use the same uniform prior for $\bar{\Xi}$ as described in the text. (Bottom) The maximum of the posterior (MAP) with the symmetric 90% credible interval about the MAP for each detector network and injected value of $\bar{\Xi}$. The credible intervals are not symmetric about the MAP when one limit of the interval reaches a boundary of the posterior. We can translate a measurement on $\bar{\Xi}$ to a measurement of the stars averaged viscosity using Eq. (5). These averaged viscosities are quoted in the abstract.

posterior distribution for $\bar{\Xi}$ for each injection. The vertical lines correspond to the injected values of $\bar{\Xi}$. Notice that $\bar{\Xi}$ is biased towards zero; we attribute this to correlations between $\bar{\Xi}$ and the tidal deformability parameters $\Lambda_{A/B}$ (see the Supp. Mat.). The one exception to this bias is the $\bar{\Xi}_{inj} = 20$ injection for the O4 network; we attribute

this increase to the fact that the spread in the posterior is very large for that network, and the injected value is close to zero (the lower bound of our prior). As expected, given the values of the SNR for the three detector networks, from Fig. (3) we see that the O5 network gives a modest improvement to the measurement of $\bar{\Xi}$. For the O4 network, we see that the posterior is mostly supported away from zero only for the largest injected value of $\bar{\Xi} = 1200$, which lies at the 90% credible interval for our current measurement from GW170817 data. In Fig. (3), we additionally present a table that shows the maximum of the posterior distribution (*maximum-a-priori* estimate, or MAP) for the recovered $\bar{\Xi}$, along with the 90% symmetric credible interval about the MAP. We see that with increasingly sensitive detectors (or alternatively, with increasingly high signal-to-noise ratio), the measurement of $\bar{\Xi}$ simultaneously becomes less biased and more precise. This is consistent with our interpretation of the bias of $\bar{\Xi}$ as arising from the correlation between $\bar{\Xi}$ and $\Lambda_{A,B}$, as those parameters simultaneously become less biased and more precise with increasing SNR as well.

Discussion We have obtained the first constraint on the dissipative tidal deformability of neutron stars, by using GW strain data from the event GW170817 as collected by the LIGO and Virgo detectors. These constraints, when mapped to bounds on the bulk viscosity, overlap with the upper end of predictions of bulk viscosity driven by Urca and hyperon processes. We have thus demonstrated that current and future GW observations of the tidal deformations of neutron stars can and have begun to inform the astrophysics, gravitational physics, and nuclear physics of out-of-equilibrium processes at supranuclear densities.

Our analysis opens the door to a plethora of future work that will be required to extract precise inferences about out-of-equilibrium microphysics. First, one must find a way to break the degeneracy between the individual dissipative tidal deformabilities $\Xi_{A,B}$, which enter the GW phase through a linear combination encapsulated in $\bar{\Xi}$. For the conservative tidal deformability $\bar{\Lambda}$, this can be done through the binary Love relations [38, 54] or through the measurement of higher post-Newtonian order terms in the phase [31, 55]. One should thus investigate the existence of similar, approximately-universal relations for the dissipative tidal deformabilities, and calculate the higher-order post-Newtonian dissipative terms. Second, the effective bulk and shear viscosities of neutron stars are predicted to depend somewhat on the stars equation of state (e.g. [18, 23, 33, 34, 48, 56–59]). Mapping inferences on $\Xi_{A,B}$ to micro-physics will thus require that one marginalize over all equations of state consistent with data, including those with sharp features in the speed of sound (e.g. [60–63]). Third, it will be critical to investigate systematic biases in parameter estimation that arise when not including the dissipative tidal effects, and statistical biases in the measurement of $\bar{\Xi}$ that arise

due to the late inspiral being buried under detector noise. Finally, the bulk and shear viscosity of neutron stars also depends sensitively on their local temperature. Connecting the individual tidal deformabilities $\Xi_{A,B}$ to nuclear physics, therefore, requires knowledge of the temperature profiles within each star, which generally increase with time (and thus with GW frequency) in the late inspiral due to tidal friction [16, 64]. This opens the possibility of learning not just about viscosity *per se*, but also about the local temperature evolution and new aspects of the equation of state of neutron stars.

Acknowledgements. We would like to thank Jorge Noronha, Jaki Noronha-Hostler, Colm Talbot, Yumu Yang, Mauricio Hippert, and Mark Alford for helpful discussions. We acknowledge support from the National Science Foundation through award PHY-2207650, and R.S.C. acknowledges support from the University of Illinois Graduate College Dissertation Completion Fellowship. We also acknowledge the Illinois Campus Cluster Program, the Center for Astrophysical Surveys (CAPS), and the National Center for Supercomputing Applications (NCSA) for the computational resources that were used to produce the results of our paper.

Supplementary material

More details of our Bayesian parameter estimation. As we mention in the main text, we sample the posterior using the nested sampling code DYNESTY. Within the Bilby interface to that code, we set `nlive=1500`, `nact=10`, `dlogz=0.01`, `sample='rwalk'`, and `bound='live'`. As a consistency check on the convergence of our sampler to the true posterior distribution, we considered runs where `nlive=1000`, `nact=5`, and `dlogz=0.1`, and found that the posterior distribution did not significantly change.

We next discuss our choice of priors in more detail. We set the chirp mass \mathcal{M} to lie within the range $[1.184M_\odot, 1.25M_\odot]$, with a distribution that is equivalent to two uniform distributions over the component masses $M_{A,B}$. The mass ratio q lies within the range $[0.5, 1]$, and is also sampled uniformly in the two component masses. We use the “low-spin” prior of [9]; that is we use uniform priors for the neutron star spins a_A, a_B over the range $[0, 0.05]$. When we sample on the tidal deformabilities separately, we use a uniform prior over the interval $[0, 3000]$ for both deformabilities. When we sample on the symmetric tidal deformability, we use a triangular prior with mean 1500 and range $[0, 3000]$. The rest of our waveform parameters follow those of [9].

We consider two separate analyses, one where we sample on the individual tidal deformabilities of the stars, $\Lambda_{A,B}$, and the symmetric tidal deformability $\Lambda_s = (\Lambda_A + \Lambda_B)/2$, from which we find $\Lambda_a = (\Lambda_A - \Lambda_B)/2$ through the binary Love relations [38]. We marginalize over the uncertainty in these relations as

described in [40, 41]. To quantify possible systematic sources of error from using a particular base waveform model, we considered two additional analyses where we added the correction Eq. (1) to two different waveform models, `IMRPhenomPv2_NRTidal` [65] and `IMRPhenomD_NRTidal` [37, 66, 67]. We found that the differences in the predictions for Ξ for all three of these models (`IMRPhenomPv2_NRTidal` with with and without the binary Love relations, and `IMRPhenomD_NRTidal` with the binary Love relations) was insignificant for GW170817 strain data.

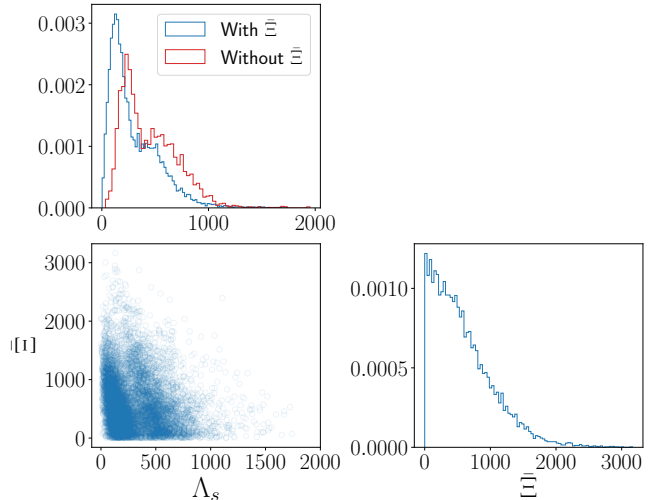


FIG. 4. Corner subspace of the marginalized posterior distribution of Λ_s and Ξ . Shown in blue are the 1-dimensional and 2-dimensional marginalized posteriors on Λ_s and Ξ corresponding to the analysis case where we do not use binary love relations. We see that the two parameters are correlated. This correlation pushes the peak of Λ_s to a slightly lower value when including Ξ in the analysis, as compared to when we exclude the Ξ correction (as is done in the LVK analysis of GW170817 [9]). Additionally shown in red in the top left panel is the 1-dimensional marginalized posterior of Λ_s from the LVK analysis where Ξ was not included (without binary love relations). We see that including Ξ pushes the marginalized posterior distribution of Λ_s to slightly lower values.

We performed an additional check on our methods by performing the same parameter estimation procedure without Ξ , and confirming that our results were statistically consistent with the LVK analysis [9] of GW170817. We note that when we include Ξ in our analysis, the peak of the marginalized posterior on Λ_s is pushed to a slightly lower value compared to when Ξ is excluded. We see from the bottom left panel of Fig. (4) that the correlation between Λ_s and Ξ is the reason for the shift of the marginalized posterior on Λ_s . That is, our agnostic analysis performed by including both conservative and dissipative tides results in slightly tighter constraints on the maximum value of the the conservative tides Λ_A and Λ_B than is obtained by the LVK analysis.

Finally, we performed another consistency check of our result for the posterior probability distribution for $\bar{\Xi}$, shown in Fig. 2, by considering different prior distributions for $\bar{\Xi}$. We considered two additional priors. We used a uniform prior in $\Xi_{A/B}$ to obtain the prior on $\bar{\Xi}$; we also sampled using a log-uniform prior on $\bar{\Xi}$. In both these cases, we find that when we divide the posterior probability distribution, multiply by our flat prior for $\bar{\Xi}$, and renormalize, we obtain a distribution statistically consistent with that shown in Fig. 2. The code we used to perform our analysis can be accessed at <https://github.com/JLRipley314/NRTidal-D>.

Estimating the significance of the tidal terms. To estimate at what frequency/radius tidal effects begin to appreciably affect the phase of emitted gravitational waves, here we compare the leading order phase contributions of the adiabatic and dissipative tides to the leading phase of a Newtonian binary of point particles. In particular, we compute the fraction p of the tidal phase with respect to the Newtonian phase for both the conservative and dissipative tidal effects. We take the fiducial value of $p = 0.025$. The leading order phase contribution for $\bar{\Xi}$ is given in Eq. (1); we recall that the leading order phasing contribution of $\tilde{\Lambda}$ is [31]

$$\Delta\Psi_{\Lambda} = -\frac{117}{256} \frac{\tilde{\Lambda}}{\eta_{\text{sym}}} u^5, \quad (6)$$

while the leading order phase contribution for a Newtonian binary of point particles is (for a review, e.g. [68])

$$\Psi_{pp} = \frac{3}{128} \frac{1}{\eta_{\text{sym}}} u^{-5}. \quad (7)$$

Setting $\Delta\Psi_{\Lambda}/\Psi_{pp} = p$, and solving for the gravitational wave frequency f (or the orbital radius r , using the relation $u^2 = GM/(rc^2)$), we obtain

$$\begin{aligned} f &\approx 467\text{Hz} \left(\frac{m}{2.8M_{\odot}}\right)^{-1} \left(\frac{p}{0.025}\right)^{3/10} \left(\frac{\tilde{\Lambda}}{575}\right)^{-3/10}, \\ r &\approx 55\text{km} \left(\frac{m}{2.8M_{\odot}}\right) \left(\frac{p}{0.025}\right)^{-1/5} \left(\frac{\tilde{\Lambda}}{575}\right)^{1/5}. \end{aligned} \quad (8)$$

For the dissipative tidal effect, setting $|\Delta\Psi_{\bar{\Xi}}/\Psi_{pp}| = p$, we solve the resulting transcendental equation numerically for f (or r),

$$-\frac{75}{32} \bar{\Xi} u^8 \log u = p. \quad (9)$$

Setting $p = 0.025$, $\bar{\Xi} = 1200$ (based on the constraint from GW170817), and $m = 2.8M_{\odot}$, we find $f \approx 253\text{Hz}$ and $r \approx 84\text{km} \sim 8R_A$. In other words, dissipative tidal effects typically become important at an earlier stage of the inspiral than conservative tidal effects. Note that for a fixed fraction p , a larger (smaller) $\bar{\Xi}$ will contribute

significantly at a lower (higher) frequency—that is the tidal effects grow stronger as the two stars in the binary move faster. If we set $\bar{\Xi} = 1200$, from $f \approx 253\text{Hz}$ until $f \approx 1569\text{Hz}$ (corresponding to the last stable orbit for $m = 2.8M_{\odot}$ mass binary), $\Delta\Psi_{\bar{\Xi}}$ accumulates 1.86 GW cycles (See Eq. (1)). For reference, over the entire inspiral (from 10Hz to 1569Hz), $\Delta\Psi_{\bar{\Xi}}$ contributes 2.5 GW cycles, while Ψ_{pp} contributes ~ 6060 GW cycles. In conclusion, most of the contribution from $\bar{\Xi}$ is accumulated during the late stage of binary inspiral.

-
- [1] W. Busza, K. Rajagopal, and W. van der Schee, *Annual Review of Nuclear and Particle Science* **68**, 339–376 (2018).
 - [2] F. Özel and P. Freire, *Ann. Rev. Astron. Astrophys.* **54**, 401 (2016), [arXiv:1603.02698 \[astro-ph.HE\]](https://arxiv.org/abs/1603.02698).
 - [3] J. M. Lattimer, *Ann. Rev. Nucl. Part. Sci.* **71**, 433 (2021).
 - [4] G. F. Burgio, H. J. Schulze, I. Vidana, and J. B. Wei, *Prog. Part. Nucl. Phys.* **120**, 103879 (2021), [arXiv:2105.03747 \[nucl-th\]](https://arxiv.org/abs/2105.03747).
 - [5] T. Hinderer, *Astrophys. J.* **677**, 1216 (2008), [arXiv:0711.2420 \[astro-ph\]](https://arxiv.org/abs/0711.2420).
 - [6] T. Damour and A. Nagar, *Phys. Rev. D* **80**, 084035 (2009), [arXiv:0906.0096 \[gr-qc\]](https://arxiv.org/abs/0906.0096).
 - [7] T. Binnington and E. Poisson, *Phys. Rev. D* **80**, 084018 (2009), [arXiv:0906.1366 \[gr-qc\]](https://arxiv.org/abs/0906.1366).
 - [8] B. P. Abbott *et al.* (LIGO Scientific, Virgo), *Phys. Rev. Lett.* **119**, 161101 (2017), [arXiv:1710.05832 \[gr-qc\]](https://arxiv.org/abs/1710.05832).
 - [9] B. P. Abbott *et al.* (LIGO Scientific, Virgo), *Phys. Rev. X* **9**, 011001 (2019), [arXiv:1805.11579 \[gr-qc\]](https://arxiv.org/abs/1805.11579).
 - [10] G. H. Darwin, *Philosophical Transactions of the Royal Society of London Series I* **170**, 1 (1879).
 - [11] G. I. Ogilvie, *Annual Review of Astronomy and Astrophysics* **52**, 171 (2014).
 - [12] J. B. Hartle, *Phys. Rev. D* **8**, 1010 (1973).
 - [13] E. Poisson, *Phys. Rev. D* **80**, 064029 (2009), [arXiv:0907.0874 \[gr-qc\]](https://arxiv.org/abs/0907.0874).
 - [14] J.-P. Zahn, *EAS Publ. Ser.* **29**, 67 (2008), [arXiv:0807.4870 \[astro-ph\]](https://arxiv.org/abs/0807.4870).
 - [15] D. Lai, *Mon. Not. Roy. Astron. Soc.* **270**, 611 (1994), [arXiv:astro-ph/9404062](https://arxiv.org/abs/astro-ph/9404062).
 - [16] P. Arras and N. N. Weinberg, *Mon. Not. Roy. Astron. Soc.* **486**, 1424 (2019), [arXiv:1806.04163 \[astro-ph.HE\]](https://arxiv.org/abs/1806.04163).
 - [17] L. Bildsten and C. Cutler, *Astrophys. J.* **400**, 175 (1992).
 - [18] R. F. Sawyer, *Phys. Rev. D* **39**, 3804 (1989).
 - [19] M. G. Alford and S. P. Harris, *Phys. Rev. C* **100**, 035803 (2019), [arXiv:1907.03795 \[nucl-th\]](https://arxiv.org/abs/1907.03795).
 - [20] M. Alford, A. Harutyunyan, and A. Sedrakian, “Bulk viscous damping of density oscillations in neutron star mergers,” (2020), [arXiv:2006.07975 \[nucl-th\]](https://arxiv.org/abs/2006.07975).
 - [21] E. R. Most, S. P. Harris, C. Plumberg, M. G. Alford, J. Noronha, J. Noronha-Hostler, F. Pretorius, H. Witek, and N. Yunes, *Mon. Not. Roy. Astron. Soc.* **509**, 1096 (2021), [arXiv:2107.05094 \[astro-ph.HE\]](https://arxiv.org/abs/2107.05094).
 - [22] M. Alford, A. Harutyunyan, and A. Sedrakian, *Particles* **5**, 361–376 (2022).
 - [23] Y. Yang, M. Hippert, E. Speranza, and J. Noronha, (2023), [arXiv:2309.01864 \[nucl-th\]](https://arxiv.org/abs/2309.01864).
 - [24] P. Hammond, I. Hawke, and N. Andersson, *Phys. Rev.*

- D **107**, 043023 (2023).
- [25] T. Celora, I. Hawke, P. Hammond, N. Andersson, and G. Comer, *Physical Review D* **105** (2022), 10.1103/physrevd.105.103016.
- [26] J. L. Ripley, A. Hegade K. R., and N. Yunes, *Phys. Rev. D* **108**, 103037 (2023), arXiv:2306.15633 [gr-qc].
- [27] M. Chabanov and L. Rezzolla, (2023), arXiv:2311.13027 [gr-qc].
- [28] M. Chabanov and L. Rezzolla, “Impact of bulk viscosity on the post-merger gravitational-wave signal from merging neutron stars,” (2023), arXiv:2307.10464 [gr-qc].
- [29] D. Radice, S. Bernuzzi, A. Perego, and R. Haas, *Monthly Notices of the Royal Astronomical Society* **512**, 1499–1521 (2022).
- [30] P. L. Espino, P. Hammond, D. Radice, S. Bernuzzi, R. Gamba, F. Zappa, L. F. L. Micchi, and A. Perego, “Neutrino trapping and out-of-equilibrium effects in binary neutron star merger remnants,” (2023), arXiv:2311.00031 [astro-ph.HE].
- [31] E. E. Flanagan and T. Hinderer, *Phys. Rev. D* **77**, 021502 (2008), arXiv:0709.1915 [astro-ph].
- [32] A. Hegade K. R., J. L. Ripley, and N. Yunes, in prep..
- [33] P. B. Jones, *Phys. Rev. D* **64**, 084003 (2001).
- [34] L. Lindblom and B. J. Owen, *Phys. Rev. D* **65**, 063006 (2002), arXiv:astro-ph/0110558.
- [35] M. G. Alford and A. Haber, *Phys. Rev. C* **103**, 045810 (2021), arXiv:2009.05181 [nucl-th].
- [36] M. E. Gusakov and E. M. Kantor, *Phys. Rev. D* **78**, 083006 (2008), arXiv:0806.4914 [astro-ph].
- [37] T. Dietrich, A. Samajdar, S. Khan, N. K. Johnson-McDaniel, R. Dudi, and W. Tichy, *Phys. Rev. D* **100**, 044003 (2019), arXiv:1905.06011 [gr-qc].
- [38] K. Yagi and N. Yunes, *Class. Quant. Grav.* **33**, 13LT01 (2016), arXiv:1512.02639 [gr-qc].
- [39] K. Yagi and N. Yunes, *Classical and Quantum Gravity* **33**, 13LT01 (2016).
- [40] K. Chatziioannou, C.-J. Haster, and A. Zimmerman, *Phys. Rev. D* **97**, 104036 (2018), arXiv:1804.03221 [gr-qc].
- [41] Z. Carson, K. Chatziioannou, C.-J. Haster, K. Yagi, and N. Yunes, *Phys. Rev. D* **99**, 083016 (2019), arXiv:1903.03909 [gr-qc].
- [42] M. Vallisneri, J. Kanner, R. Williams, A. Weinstein, and B. Stephens, *J. Phys. Conf. Ser.* **610**, 012021 (2015), arXiv:1410.4839 [gr-qc].
- [43] J. D. E. Creighton and W. G. Anderson, *Gravitational-wave physics and astronomy: An introduction to theory, experiment and data analysis* (2011).
- [44] M. Coleman Miller and N. Yunes, *Gravitational Waves in Physics and Astrophysics* (IOP, 2021).
- [45] G. Ashton *et al.*, *Astrophys. J. Suppl.* **241**, 27 (2019), arXiv:1811.02042 [astro-ph.IM].
- [46] J. Skilling, *Bayesian Analysis* **1**, 833 (2006).
- [47] J. S. Speagle, *Mon. Not. R. Astron. Soc* **493**, 3132 (2020), arXiv:1904.02180 [astro-ph.IM].
- [48] P. S. Shternin and D. G. Yakovlev, *Phys. Rev. D* **78**, 063006 (2008), arXiv:0808.2018 [astro-ph].
- [49] C. S. Kochanek, *Astrophys. J.* **398**, 234 (1992).
- [50] A. Perego, S. Bernuzzi, and D. Radice, *Eur. Phys. J. A* **55**, 124 (2019), arXiv:1903.07898 [gr-qc].
- [51] M. G. Alford, A. Haber, and Z. Zhang, (2023), arXiv:2306.06180 [nucl-th].
- [52] B. P. Abbott *et al.* (KAGRA, LIGO Scientific, Virgo, VIRGO), *Living Rev. Rel.* **21**, 3 (2018), arXiv:1304.0670 [gr-qc].
- [53] B. P. Abbott *et al.* (LIGO Scientific), *Class. Quant. Grav.* **34**, 044001 (2017), arXiv:1607.08697 [astro-ph.IM].
- [54] K. Yagi and N. Yunes, *Class. Quant. Grav.* **34**, 015006 (2017), arXiv:1608.06187 [gr-qc].
- [55] J. Vines, E. E. Flanagan, and T. Hinderer, *Phys. Rev. D* **83**, 084051 (2011), arXiv:1101.1673 [gr-qc].
- [56] P. Haensel, K. P. Levenfish, and D. G. Yakovlev, *Astron. Astrophys.* **357**, 1157 (2000), arXiv:astro-ph/0004183.
- [57] E. Flowers and N. Itoh, *Astrophys. J.* **206**, 218 (1976).
- [58] E. Flowers and N. Itoh, *Astrophys. J.* **230**, 847 (1979).
- [59] B. T. Goodwin and C. J. Pethick, *Astrophys. J.* **253**, 816 (1982).
- [60] H. Tan, J. Noronha-Hostler, and N. Yunes, *Phys. Rev. Lett.* **125**, 261104 (2020), arXiv:2006.16296 [astro-ph.HE].
- [61] H. Tan, V. Dexheimer, J. Noronha-Hostler, and N. Yunes, *Phys. Rev. Lett.* **128**, 161101 (2022), arXiv:2111.10260 [astro-ph.HE].
- [62] H. Tan, T. Dore, V. Dexheimer, J. Noronha-Hostler, and N. Yunes, *Phys. Rev. D* **105**, 023018 (2022), arXiv:2106.03890 [astro-ph.HE].
- [63] D. Mroczek, M. C. Miller, J. Noronha-Hostler, and N. Yunes, (2023), arXiv:2309.02345 [astro-ph.HE].
- [64] D. Lai, *Mon. Not. R. Astron. Soc* **270**, 611 (1994), arXiv:astro-ph/9404062 [astro-ph].
- [65] T. Dietrich *et al.*, *Phys. Rev. D* **99**, 024029 (2019), arXiv:1804.02235 [gr-qc].
- [66] S. Husa, S. Khan, M. Hannam, M. Pürrer, F. Ohme, X. Jiménez Forteza, and A. Bohé, *Phys. Rev. D* **93**, 044006 (2016), arXiv:1508.07250 [gr-qc].
- [67] S. Khan, S. Husa, M. Hannam, F. Ohme, M. Pürrer, X. Jiménez Forteza, and A. Bohé, *Phys. Rev. D* **93**, 044007 (2016), arXiv:1508.07253 [gr-qc].
- [68] M. Maggiore, *Gravitational Waves: Volume 1: Theory and Experiments* (Oxford University Press, 2007).